JOURNAL OF THERMOPHYSICS AND HEAT TRANSFER
Vol. 20, No. 2, April–June 2006

Stabilization of Ill-Posed Problems Through Thermal Rate Sensors

J. I. Frankel* and G. E. Osborne†
University of Tennessee, Knoxville, Tennessee 37996-2210
and
K. Taira‡
California Institute of Technology, Pasadena, California 91125

Reliance on conventional temperature and heat flux sensors in transient situations can inhibit predictiveness and lead to unsatisfactory results that require extensive post-processing procedures for reconstituting usable results. A mathematical formalism is presented to motivate the development of thermal rate sensors. Rate-based temperature and heat flux sensors can be designed in a manner without requiring any form of data differentiation. The proposed temperature and heat flux rate sensors can enhance both real-time and postprocessing investigations. A new sensor hierarchy is proposed that reduces and, in some cases, removes the often encountered ill-posed nature observed in numerous heat transfer studies. Four diverse examples are presented illustrating the power of rate-based data for enhancing stability and accuracy. Numerical regularization that is normally required for assuring stability can effectively be eliminated by data from thermal rate sensors. Additionally, in some investigations, these data forms can assist in identifying optimal regularization parameters. Data from rate-based sensors can make an immediate impact on a variety of aerospace, defense, and material science studies.

Nomenclature

A	=	constant, °C/s^3
C	=	heat capacity, kJ/(kg°C)
D	=	differential operator, $\partial/\partial t$
$f(t)$	=	specified temperature function, Eq. (15b)
G	=	Green's function, Eq. (2b)
$g(t)$	=	specified heat flux function, Eq. (15c)
H	=	Heaviside step function, Eq. (8d)
K	=	integral operator, Eq. (3b)
k	=	thermal conductivity, W/(m°C)
L	=	fixed position, m
M	=	number of data points
N	=	number of space terms
N_j	=	difference norm, Eq. (20)
P	=	number of time terms
p_{opt}	=	optimal number of temporal terms
Q	=	dimensionless heat flux
Q_{NP}	=	approximate heat flux
q''	=	dimensional heat flux, W/m^2
q''_i	=	discrete heat flux, W/m^2
$\dot{q}''_i$	=	discrete heat flux rate, W/(m^2 s)
$q''_{\max}$	=	maximum heat flux, W/m^2
$s(t)$	=	location of moving front, m
T	=	temperature, °C
T_i	=	discrete temperature, °C
$\dot{T}_i$	=	discrete heating/cooling rate, °C/s
$\ddot{T}_i$	=	discrete second time derivative of temperature, °C/s^2
T_{melt}	=	melt temperature, °C
$T_m(\chi)$	=	mth Chebyshev polynomial of the first kind
T_0	=	initial temperature, °C
t	=	time, s
t_j	=	discrete time, s
$t_{\max}$	=	maximum time, s
t_{pen}	=	penetration time, s
t_0	=	dummy variable, s
x	=	spatial variable, m
x_0	=	dummy variable, m
α	=	thermal diffusivity, m^2/s
β	=	shape factor
γ	=	constant in definition of penetration time
ϵ_i	=	imposed noise level, Eq. (6)
η	=	fixed position
θ	=	dimensionless temperature
θ_i	=	dimensionless discrete temperature
$\dot{\theta}_i$	=	dimensionless discrete heating/cooling rate
λ	=	constant $[1/\sqrt{(k\rho C\pi)}]$
λ_0	=	$t_{\max}/2$, s
ξ	=	Chebyshev temporal coordinate
ρ	=	density, kg/m^3
σ_i	=	noise level, Eq. (17)
χ	=	Chebyshev spatial coordinate
Ω_{mn}	=	trial function defined, Eq. (18a)
ω_i	=	noise level, Eq. (13)
$\omega_m(\chi)$	=	spatial trial function, Eq. (18c)

Received 15 March 2004; revision received 19 August 2004; accepted for publication 26 September 2004.

*Professor, Mechanical, Aerospace, and Biomedical Engineering Department. Senior Member AIAA.

†Ph.D. Candidate, Mechanical, Aerospace, and Biomedical Engineering Department. Member AIAA.

‡Ph.D. Candidate, Mechanical Engineering, Mail Code 104-44, 1200 East California Boulevard. Student Member AIAA.

Introduction

HEAT transfer analysis often involves the precise measurement of temperature and heat flux.[1–4] These quantities have been traditionally sought, and numerous sensors have been developed, capable of producing accurate results over various conditions, applications, and thermal ranges. High-temperature, heat fluxes, and heating/cooling rates are of practical concern because of their appearance in aerospace, defense, and nuclear applications. Reentry and direct-energy impingement are high-temperature and heat flux applications. Additionally, short-time duration applications are appearing in great quantity. For example, arcjets[3] used to simulate reentry heat transfer tend to run only for a few seconds. Also, directed energy deposition on objects may last for short durations. Note that Neumann et al.[4] stated in 1988 that instrumentation in hypersonic structures has been "terribly flawed" in the previous decades.

Applications can be subdivided into real-time requirements or postprocessing analysis. Diagnostics and evaluation applications

collect data that can be analyzed at a later time to evaluate thermophysical properties or deduce surface heat fluxes from measured temperatures. In contrast, health monitoring and control may require real-time analysis from which immediate decisions can be made. For example, the appearance of a sudden hot spot at a surface will require an immediate action to cool a specific location in an intelligent and rapid manner. The local energy content, as well as temperature, are required for a corrective action to transpire.

Several basic requirements for developing the accurate capture and interpretation of data consistently appear. In particular, the need exists for developing methods that permit the quantitative evaluation of local errors and new real-time intrusive and nonintrusive measurement techniques for application in highly hostile environments. Embedded sensors are used to deduce or project to the location of interest when direct surface probe placement is not possible. This often leads to ill-posed problems in which error amplification will most certainly dominate.[5–8] Inverse problems are termed ill-posed in the sense used by Hadamard because a small perturbation in the input can produce randomly large variations in the output. The word input here is related to the state variable or solution.

This situation is unlike the analysis of direct problems in that a small perturbation in the input produces a small perturbation in the output. Note that numerical differentiation of discrete, noisy data represents the most fundamental ill-posed problem.[9–11] Numerical differentiation of noisy data is known to be ill-posed in the sense used by Hadamard because small perturbations in the function can lead to large variations in the derivative. This can quickly be understood by noting that the absolute error associated with a forward difference approximation to $f'_\epsilon(x)$ in the presence of noisy data results in the error bound $f'_\epsilon < \mathcal{O}(h) + 2\delta/h$, where δ is the maximum absolute error, that is, $|f - f_i| < \delta$, and h is the conventional step size. Therefore, for $\delta > 0$, as $h \to 0$, the resulting error bound blows up. Thus, $h \to 0$ cannot be performed in an arbitrary manner.

In transient heat transfer situations, it is well known that the order of the differential equation (in time) gives insight into the best form of data to be collected. However, this important mathematical fact is often put aside in lieu of using traditional sensors based on temperature and heat flux. For example, the transient heat equation expressed in temperature is first order in time. Thus, if data were presented in heating/cooling rate terms ($\mathrm{d}T/\mathrm{d}t$), the severity of the ill-posed nature is basically reduced.[12–16] Changing the data space can effectively remove the ill-posed nature. Direct differentiation of data by coarse grid regularization[9,10] or other such methods may require the removal of physically important data. Several methods[5–8] involving some form of Tikhonov regularization have also been developed.

Example Based Study

A motivational approach is presented to illustrate that numerical stabilization can be achieved by choosing the appropriate data space. Apparently, though known to mathematicians, most engineering studies have persisted in devising a purely numerical approach relying on some sort of regularization. The optimal regularization parameter is often elusive, and no steadfast mathematical rule exists for assuring the optimal prediction. This paper presents several compelling examples that clearly elucidate the need for a rate-based sensor solution. A slightly unconventional format is chosen to relate the four diverse examples under consideration.

Example 1: Half-Space Heat Conduction

A common mathematical formulation appearing in heat transfer[17–20] involves the half-space heat conduction problem. This example is briefly described and is shown to be ill-posed in the sense used by Hadamard, even though only a single spatial point is involved as time evolves. Actually, note that numerous investigators in the past have failed to understand the ill-posed nature of the problem. Inherent to this study is the differentiation of noisy data. Linz's,[21] pp. 207–211 classical example involving a Volterra integral equation of the first kind indicates the problem associated with discrete data in the primitive variable. It is obvious that unlike second-kind integral equations, no upper bound on the error exists. This is a consequence of an ill-posed problem. Baker,[22] Golberg,[23] Wing,[6] and Kress[5] have noted that usually low-order quadrature rules are used and some form of extrapolation or smoothing is needed to provide accuracy and to control high-frequency oscillations in the numerically acquired values.

For illustration purposes, consider the linear (constant property) heat equation for the half-space problem. The heat equation is given by

$$\frac{1}{\alpha}\frac{\partial T}{\partial t}(x,t) = \frac{\partial^2 T}{\partial x^2}(x,t), \qquad x \geq 0, \qquad t \geq 0 \tag{1a}$$

where x and t represent the spatial and temporal variables, respectively. The thermal diffusivity is $\alpha = k/(\rho C)$, where k is the thermal conductivity, ρ is the density, and C is the heat capacity. This field equation is subject to the initial (equilibrium) condition

$$T(x,0) = T_0, \qquad x \geq 0 \tag{1b}$$

Without loss of generality, let $T_0 = 0$, and, presently, no explicit boundary condition at $x = 0$ is specified. The conventional relationship between temperature and heat flux is given by Fourier's law

$$q''(x,t) = -k\frac{\partial T}{\partial x}(x,t) \tag{1c}$$

which follows classical assumptions associated with parabolic heat conduction.[24,25] An equivalent integral equation can be devised based on a boundary element approach.[26] To this end, one can obtain

$$w(x)T(x,t) = -\int_{t_0=0}^{t}\left[G(x,t/0,t_0)\frac{\partial T}{\partial x_0}(0,t_0) - \frac{\partial G}{\partial x_0}(x,t/0,t_0)T(0,t_0)\right]\mathrm{d}t_0, \qquad x,t \geq 0 \tag{2a}$$

where $w(x)$ is a weight function [$w(0) = 0.5$, $w(x) = 1$ for $x \neq 0$], and the full-space Green's function is given by

$$G(x,t/x_0,t_0) = \sqrt{\frac{\alpha}{4\pi(t-t_0)}}\exp\left[\frac{-(x-x_0)^2}{4\alpha(t-t_0)}\right]$$
$$(x,x_0) \in (-\infty,\infty), \qquad t > t_0 \tag{2b}$$

Evaluating Eq. (2a) at $x = 0$ produces

$$T(0,t) = \lambda\int_{t_0=0}^{t}\frac{q''(0,t_0)}{\sqrt{t-t_0}}\,\mathrm{d}t_0 = \lambda K q'', \qquad t \geq 0 \tag{3a}$$

because $q''(0,t) = -k(\partial T/\partial x)(0,t)$ and $\lambda = 1/\sqrt{(k\rho C\pi)}$. Here, the integral operator K is defined as

$$Kb = \int_{t_0=0}^{t}\frac{b(t_0)}{\sqrt{t-t_0}}\,\mathrm{d}t_0, \qquad t \geq 0 \tag{3b}$$

Equation (3) is an Abel integral equation (see Refs. 21–23) for $q''(0,t)$. This equation permits inversion when provided $T(0,t)$ by a conventional approach involving regularization (as associated with singular integral equations and not ill-posed problems).

Inversion of Eq. (3a) produces the deceivingly simple result of

$$q''(0,t) = \frac{1}{\lambda\pi}\int_{t_0=0}^{t}\frac{(\partial T/\partial t_0)(0,t_0)}{\sqrt{t-t_0}}\,\mathrm{d}t_0 = \frac{1}{\lambda\pi}K(DT)$$
$$t \geq 0 \tag{4}$$

where D represents the conventional differential operator defined as $D = \partial/\partial t$. This equation reveals that if data are collected in the (primitive variable) temperature $T(0,t)$, then its time derivative is required. When data are discrete and noisy, the task is problematic. Integration by parts applied to Eq. (4) does not remove or deter the

true nature of the problem. Also note that Eqs. (3a) and (4) can be elegantly expressed in terms of fractional derivatives.

The Abel system given in Eqs. (3a) and (4) has infinite inversion properties. This observation has received little or no attention. That is, one can continue to form a logical sequence of higher-time derivative solutions involving both the temperature and heat flux. This process leads to a roadmap that describes the coupling between stability and the data space. The following Abel sequence is obtained using the general and well-known inversion property (see Refs. 21–23) of the Abel equation, namely,

$$\frac{\partial T}{\partial t}(0,t)=\lambda\int_{t_0=0}^{t}\frac{(\partial q''/\partial t_0)(0,t_0)}{\sqrt{t-t_0}}\,\mathrm{d}t_0=\lambda K(Dq'') \qquad t\geq 0 \quad (5a)$$

$$\frac{\partial q''}{\partial t}(0,t)=\frac{1}{\lambda\pi}\int_{t_0=0}^{t}\frac{(\partial^2 T/\partial t_0^2)(0,t_0)}{\sqrt{t-t_0}}\,\mathrm{d}t_0=\frac{1}{\lambda\pi}K(D^2T) \qquad t\geq 0 \quad (5b)$$

$$\frac{\partial^2 T}{\partial t^2}(0,t)=\lambda\int_{t_0=0}^{t}\frac{(\partial^2 q''/\partial t_0^2)(0,t_0)}{\sqrt{t-t_0}}\,\mathrm{d}t_0=\lambda K(D^2q'') \qquad t\geq 0,\ldots \quad (5c)$$

This form leads to a stability roadmap that will be described shortly.

The true behavior of the Abel system given in Eqs. (3a) and (4) is now numerically considered. For definiteness, a simple problem is devised such that $T(0,t)=A(t_{\max}t^2/2-t^3/3)$, and, thus, $q''(0,t)=-(4/15)At^{1.5}(4t-5t_{\max})\sqrt{(\rho Ck/\pi)}$. For the present simulation, let $A=600^\circ C/s^3$ and $t_{\max}=2.5$ s. Artificial test data containing only random error are generated by

$$T_i=T(0,t_i)+\|T(0,t)\|_\infty\epsilon_1\,\mathrm{rand}_{1,i} \quad (6a)$$

$$\dot{T}_i=\frac{\mathrm{d}T_i}{\mathrm{d}t}=\frac{\partial T}{\partial t}(0,t_i)+\left\|\frac{\partial T}{\partial t}\right\|_\infty\epsilon_2\,\mathrm{rand}_{2,i}, \qquad i=1,2,\ldots,M \quad (6b)$$

where ϵ_j, $j=1,2$, denotes the noise factor; $\mathrm{rand}_{j,i}$, $j=1,2$, $i=1,2,\ldots,M$, is a randomly drawn number in the interval $[-1,1]$, and M is the total number of data in the set. The uniform norm of the function $f(t)$ is defined as $\|f(t)\|_\infty=\max_{t\epsilon[0,t_{\max}]}|f(t)|$, where $t_{\max}$ is the maximum amount of time data are collected. The dot derivative notation is used throughout this paper for representating discrete data. Equation (4) is often discretized using the Cook–Felderman approach[19] (see also Refs. 17 and 20), which relies on the availability of temperature data. In accordance to this method, the discretized form becomes

$$q_i''=\frac{1}{\lambda\pi}\left[\frac{T_i}{\sqrt{t_i}}+\sum_{j=1}^{i-1}\left(\frac{T_i-T_j}{\sqrt{t_i-t_j}}-\frac{T_i-T_{j-1}}{\sqrt{t_i-t_{j-1}}}+\frac{2(T_j-T_{j-1})}{\sqrt{t_i-t_j}+\sqrt{t_i-t_{j-1}}}\right)+\frac{T_i-T_{i-1}}{\sqrt{t_i-t_{i-1}}}\right] \qquad i=1,2,\ldots,M \quad (7a)$$

Under the supposition that $\{\dot{T}_i\}_{i=1}^M$ data are available, let us discretize Eq. (4) by the most primitive integration rule (left-side, product-rectangular rule[21]) to obtain

$$q_i''=\frac{2}{\lambda\pi}\sum_{j=0}^{i-1}\frac{\mathrm{d}T_j}{\mathrm{d}t}\left(\sqrt{t_i-t_j}-\sqrt{t_i-t_{j+1}}\right), \qquad i=1,2,\ldots,M \quad (7b)$$

Figure 1 shows the created data sets for both T_i and $\dot{T}_i$, where $\epsilon_1=0.05$, $\epsilon_2=3\epsilon_1$, and $M=100$. The solid lines indicate the exact function from which the data are generated. For this example, the required thermophysical properties used in Eq. (7) are taken for copper at 800 K [$\rho=8933\,\mathrm{kg/m^3}$, $C=433\,\mathrm{kJ/(kgK)}$, and $k=366\,\mathrm{W/(mK)}$]. Figure 2 shows the results of the simulations based on a) the Cook–Felderman method (raw data), b) the Cook–Felderman method [data corrected using the method of Frankel–Keyhani–Taira[11] (F–K–T)], and c) left-hand rectangular rule (raw $\dot{T}_i$ data).

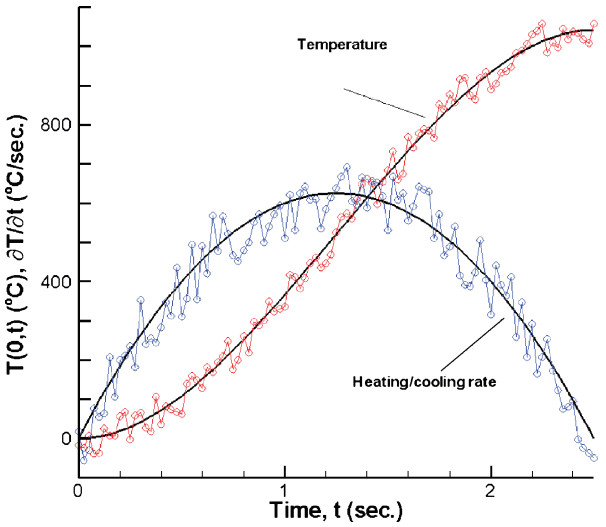

Fig. 1 Data: ——, exact and ○, simulated, for T (red) and $\dot{T}$ (blue).

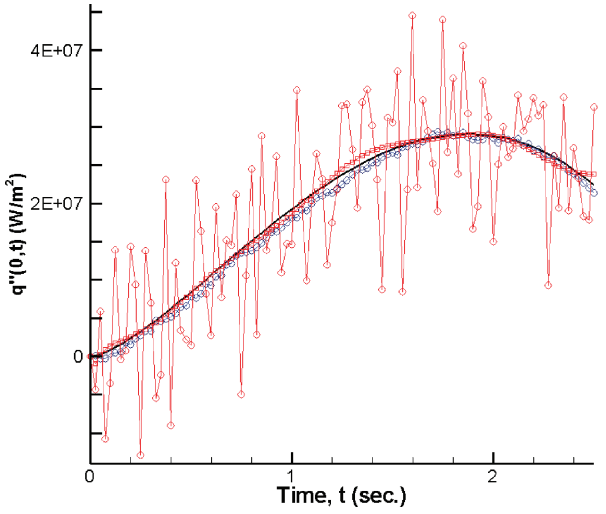

Fig. 2 Resulting heat fluxes using T: ○, red, raw data; □, red, corrected data[11]; and ○, blue, raw data.

The direct integration of the raw $\dot{T}_i$ data produces a stable and accurate prediction for flux using Eq. (7b). With no a priori error analysis, $\dot{T}_i$ permits real-time evaluation of $q''(0,t)$ by direct integration. The heat flux is shown to be insensitive to large errors in $\dot{T}_i$. Again, the heating/cooling rate data noise level is significantly higher than the induced error level in the temperature data. For this example, with a known solution, the flux is lower than the expected value until nearing the peak due to the left-hand biasing of the integrator. Notice that past the maximum value, the calculated flux begins to correct itself as necessitated by the bias. This distraction can be corrected by changing the quadrature rule. The Cook–Felderman method works well if T_i data are preprocessed using the F–K–T method.[11]

A clear explanation of the mathematical sequence described in Eq. (5) is now presented. Figure 3 presents the path of stability (in the presence of random error) for resolving the desired thermal quantity based on the data space. The columns of the graphical structure, containing the D and D^{-1} operators, point out the well- and

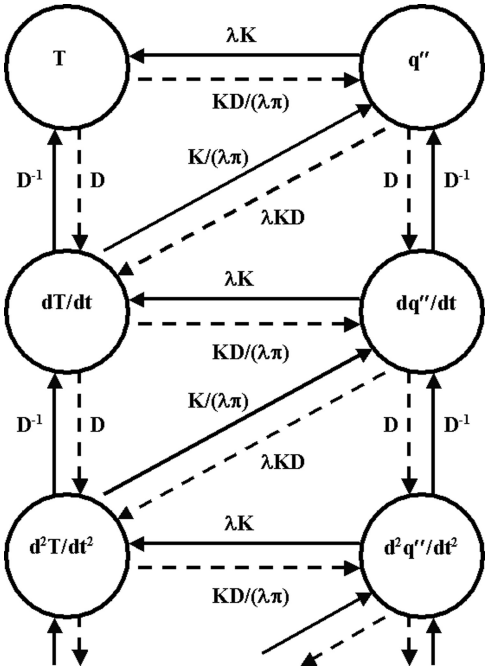

Fig. 3 Stabilized procedure based on data space infinite Abel integral transform pairing: ○, data space; - - - -, ill posed; and ——, well posed.

ill-posed directions of integration and differentiation, respectively. The horizontal and diagonal components describe the physical problem composed of the particular and general laws of classical heat conduction. That is, it appears that the proper choice of collected data can remove the need for mathematical regularization methods. Regularization methods do not offer definitive metrics for optimal predictions. It is indicated in Fig. 3 that the stable calculation of the heat flux is available based on heating/cooling rate data (dT/dt), as seen in Eq. (4). This is verified by the numerical results given in Fig. 2. The clear sequencing indicates the desired input rate data for producing a stable output.

Example 2: Real-Time Surface Predictions from Embedded Sensors

This example addresses the question as to what the most suitable transient sensors are for resolving inverse heat conduction problems in a real-time basis. The approach taken here is based on analytic continuation (Taylor series). Consider the constant property heat equation in the half-space given as

$$\frac{1}{\alpha}\frac{\partial T}{\partial t}(x,t) = \frac{\partial^2 T}{\partial x^2}(x,t), \qquad x \geq 0, \qquad t \geq 0 \tag{8a}$$

subject to the time-dependent boundary condition

$$-k\frac{\partial T}{\partial x}(0,t) = q''(t), \qquad t \geq 0 \tag{8b}$$

and initial condition

$$T(x,0) = T_0, \qquad x \geq 0 \tag{8c}$$

where the heat flux $q''(t)$ is given by

$$q''(t) = q''_{\max}\sum_{j=0}^{N} H(t-t_j)(-1)^j, \qquad t \geq 0 \tag{8d}$$

Here, x is the x-coordinate, $q''_{\max}$ is the maximum heat flux in each step function, and $H(z)$ is the Heaviside function. Equation (8d) describes the applied stepwise surface heat flux where the time set $\{t_j\}_{j=0}^{N}$ describes the various breakpoints used to define the pulse width and delay time between thermal events. This boundary condition represents a critical test for the proposed concept due to its abruptive behavior.

The exact solution can be obtained by conventional methods to yield

$$T(x,t) = \frac{q''_{\max}\sqrt{\alpha}}{k}\sum_{j=0}^{N}(-1)^j\left\{\frac{\sqrt{4(t-t_j)}}{\sqrt{\pi}}\exp\left[\frac{-x^2}{4\alpha(t-t_j)}\right] - \frac{x}{\sqrt{\alpha}}\operatorname{erfc}\left(\frac{x}{\sqrt{4\alpha(t-t_j)}}\right)\right\}H(t-t_j), \qquad x,t \geq 0 \tag{9}$$

where $\operatorname{erfc}(z)$ is the complementary error function.

Next, using the concept of analytic continuation, that is, Taylor series, one can expose important sensor contributions. To begin, a half-space region is defined containing the embedded location denoted as $x = \eta$. Consider the Taylor series expansion of the function $T(x,t)$ about the embedded point $x = \eta > 0$, namely,

$$T(0,t) = T(\eta,t) - \frac{\partial T}{\partial x}(\eta,t)\frac{\eta}{1!} + \frac{\partial^2 T}{\partial x^2}(\eta,t)\frac{\eta^2}{2!} - \frac{\partial^3 T}{\partial x^3}(\eta,t)\frac{\eta^3}{3!} + \frac{\partial^4 T}{\partial x^4}(\eta,t)\frac{\eta^4}{4!}\cdots \tag{10}$$

For the moment, this formulation does not include any thermal lag due to delay (penetration as defined by the estimation $t_{\text{pen}} = \eta^2/\gamma\alpha$, where γ is a constant). The classical penetration time is dependent on length and thermal diffusivity. For the moment, it is assumed that $t_{\text{pen}} \approx 0$. Equation (10) can be alternatively expressed in various temporal derivatives of the temperature $T(x,t)$ and heat flux $q''(x,t)$ through the particular law describing Fourier's heat conduction $q''(x,t) = -k(\partial T/\partial x)$ and the first law of thermodynamics given by $\rho C(\partial T/\partial t) = -(\partial q''/\partial x)$. That is, one can express Eq. (10) as

$$T(0,t) = T(\eta,t) + q''(\eta,t)\frac{\eta}{1!k} + \frac{\partial T}{\partial t}(\eta,t)\frac{\eta^2}{2!\alpha} + \frac{\partial q''}{\partial t}(\eta,t)\frac{\eta^3}{3!\alpha k} + \frac{\partial^2 T}{\partial t^2}(\eta,t)\frac{\eta^4}{4!\alpha^2} + \frac{\partial^2 q''}{\partial t^2}(\eta,t)\frac{\eta^5}{5!\alpha^2 k} + \frac{\partial^3 T}{\partial t^3}(\eta,t)\frac{\eta^6}{6!\alpha^3} + \frac{\partial^3 q''}{\partial t^3}(\eta,t)\frac{\eta^7}{7!\alpha^3 k} + \cdots \tag{11}$$

Equation (11) encourages the measurement of $T(\eta,t)$, $q''(\eta,t)$, and their temporal derivatives. The continuation effect and the formation of accurate projections are illustrated with the aid of Fig. 4 [$T(0,t)$ = exact, $T1$ = One-term Taylor, $T2$ = Two-term Taylor, etc.], using properties associated with copper as noted earlier and where $\eta = 0.635$ cm. The projection is reconstructed within a few terms.

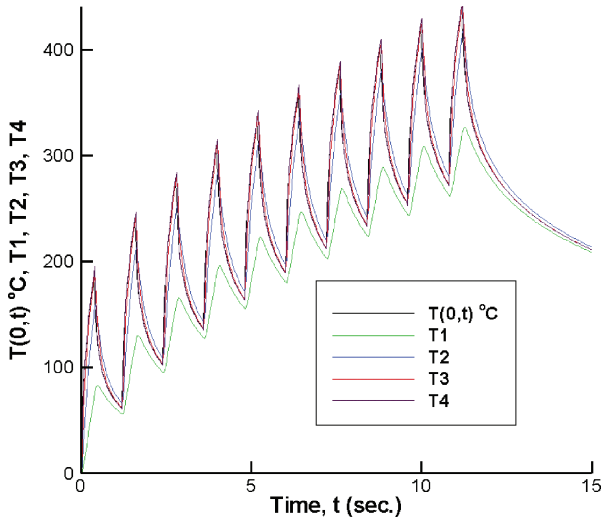

Fig. 4 Taylor approximation of $T(0,t)$ as additional terms are retained, for copper: $\alpha = 117 \times 10^{-6}$ m²/s, $k = 401$ W/(mK), $T_0 = 0$°C, and $\eta = 0.635$ cm.

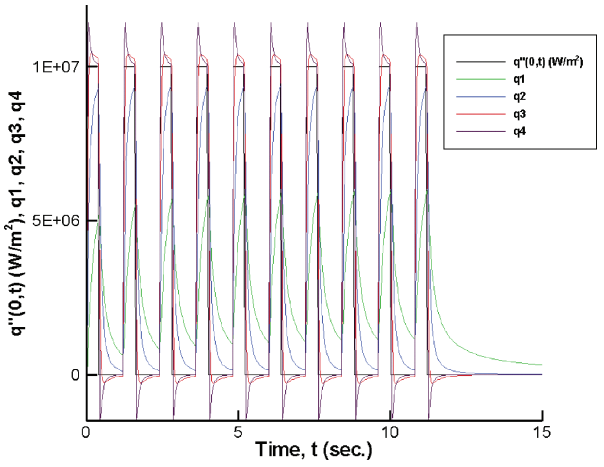

Fig. 5 Taylor approximation of $q''(0, t)$ as additional terms are retained, for copper: $\alpha = 117 \times 10^{-6}$ m^2/s, $k = 401$ W/(mK), $T_0 = 0°$C, and $\eta = 0.635$ cm.

A similar Taylor series can be developed for $q''(0, t)$ based on measured rate quantities at $x = \eta$. In this case, one obtains

$$q''(0,t) = q''(\eta,t) + \frac{k}{\alpha}\frac{\partial T}{\partial t}(\eta,t)\frac{\eta}{1!} + \frac{1}{\alpha}\frac{\partial q''}{\partial t}(\eta,t)\frac{\eta^2}{2!} + \frac{k}{\alpha^2}\frac{\partial^2 T}{\partial t^2}(\eta,t)\frac{\eta^3}{3!} + \frac{1}{\alpha^2}\frac{\partial^2 q''}{\partial t^2}(\eta,t)\frac{\eta^4}{4!} + \cdots \tag{12}$$

Figure 5 displays partial sums of the heat flux expansion shown in Eq. (12). Note that four terms [$q''(0, t) =$ exact, $q1 =$ One-term Taylor, $q2 =$ Two-term Taylor, etc.] are utilized under the present assumption of five available sensors because $T(\eta, t)$ is not explicitly required. It is surprising to see how well the discontinuous nature of the heat flux is reconstructed using a mere Taylor series. Equations (11) and (12) strongly suggest that a series of rate-based sensors involving T and q'' be developed.

The real value of this concept must be evaluated using noisy data at the probe location. To emulate noisy data, let

$$T_i = T(\eta, t_i)(1 + \omega_1 \,\mathrm{rand}_{1,i}) \tag{13a}$$

$$q_i'' = q''(\eta, t_i)(1 + \omega_2 \,\mathrm{rand}_{2,i}) \tag{13b}$$

$$\dot{T}_i = \frac{\partial T}{\partial t}(\eta, t_i)(1 + \omega_3 \,\mathrm{rand}_{3,i}) \tag{13c}$$

$$\dot{q}_i'' = \frac{\partial q''}{\partial t}(\eta, t_i)(1 + \omega_4 \,\mathrm{rand}_{4,i}) \tag{13d}$$

$$\ddot{T}_i = \frac{\partial^2 T}{\partial t^2}(\eta, t_i)(1 + \omega_5 \,\mathrm{rand}_{5,i}) \tag{13e}$$

where ω_j, $j = 1{-}5$, denotes the noise factor, $\mathrm{rand}_{j,i}$, $j = 1{-}5$, $i = 1, 2, \ldots, M$, are randomly drawn numbers from the interval $[-1, 1]$, and M is sample data size. Figures 6–9 present results for the surface temperature and heat flux using copper and iron, where $\eta = 0.3175$ cm. Iron is a poor thermal conductor and, as such, represents a good contrast to the copper results.

Figures 6 and 7 present the reconstructed surface temperature and heat flux in a copper body using the simulated data described in Eq. (13). These data are substituted into the right-hand sides of Eqs. (11) and (12). For this simulation, $\omega_1 = 0.05$ and $\omega_j = 2\omega_{j-1}$, $j = 2, 3, 4, 5$; the pulse width is 0.8 s; and delay time between pulses is 1.6 s, leading to seven pulses in the 15-s time span. That is, it is assumed that the error increases in the sensor for each derivative and that greater error is present in the flux measurement than temperature measurement. The error is clearly additive, and, thus, the projection is stable. Only a few terms are required to reconstruct the desired surface condition. The accuracy of the projection increases as additional terms are included. A significant local error has been

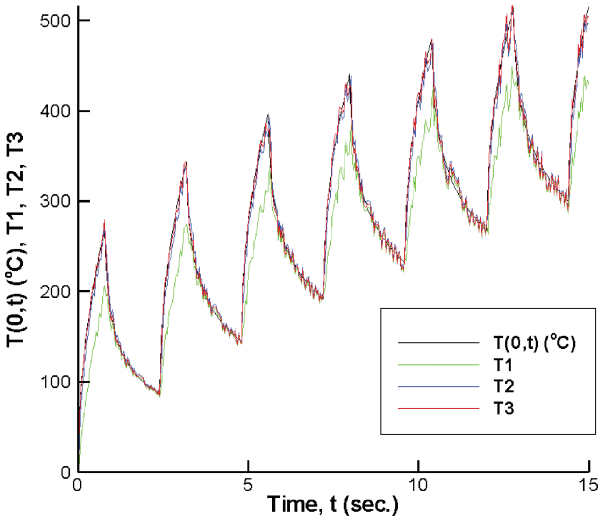

Fig. 6 Taylor approximation of $T(0, t)$ as additional terms are retained in the presence of noisy data, for copper: $\alpha = 117 \times 10^{-6}$ m^2/s, $k = 401$ W/(mK), $T_0 = 0°$C, and $\eta = 0.3175$ cm.

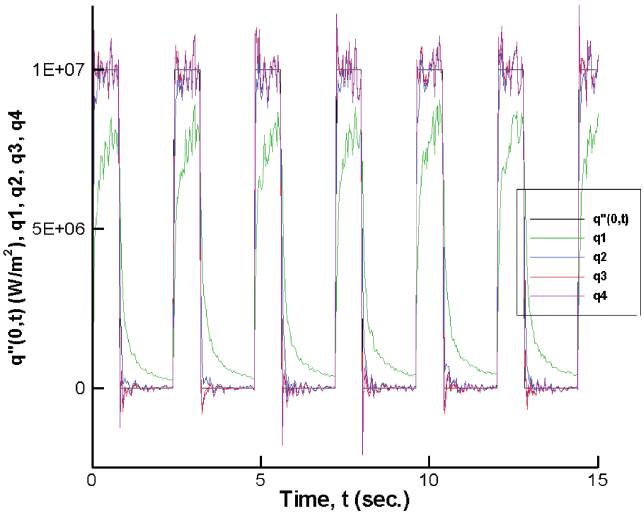

Fig. 7 Taylor approximation of $q''(0, t)$ as additional terms are retained in the presence of noisy data, for copper: $\alpha = 117 \times 10^{-6}$ m^2/s, $k = 401$ W/(mK), $T_0 = 0°$C, and $\eta = 0.3175$ cm.

introduced into the higher-order sensors (Taylor terms). For copper, these terms are not significant. The actual error decomposition leads to local errors in the measurement sensor and the truncation error of the Taylor series.

Figures 8 and 9 present the reconstructed surface temperature and heat flux for an iron body using the simulated data described in Eq. (13). For this simulation, $\omega_1 = 0.05$ and $\omega_j = 2\omega_{j-1}$, $j = 2, 3, 4, 5$. The heat flux is reconstructed in a fairly accurate form considering the nature of the imposed flux condition. Iron requires more terms than copper in the reconstruction process because of its lower thermophysical properties.

Lagging effects in the projection are visually apparent as η increases beyond some threshold value. It is possible to include this effect into the Taylor series. For the moment, assume that the penetration time, t_{pen} can be expressed as $t_{\mathrm{pen}} = \eta^2/(\gamma\alpha)$, where γ is a constant. Penetration times may be experimentally estimated if required. The multivariable Taylor series (see Ref. 27, p. 439) for the surface temperature up to $\mathcal{O}(\eta^3)$ is

$$T(0, t - t_{\mathrm{pen}}) = T(\eta,t) + q''(\eta,t)\frac{\eta}{1!k} + \frac{\partial T}{\partial t}(\eta,t)\left(\frac{\eta^2}{2!\alpha} - t_{\mathrm{pen}}\right) + \mathcal{O}(\eta^3) \tag{14a}$$

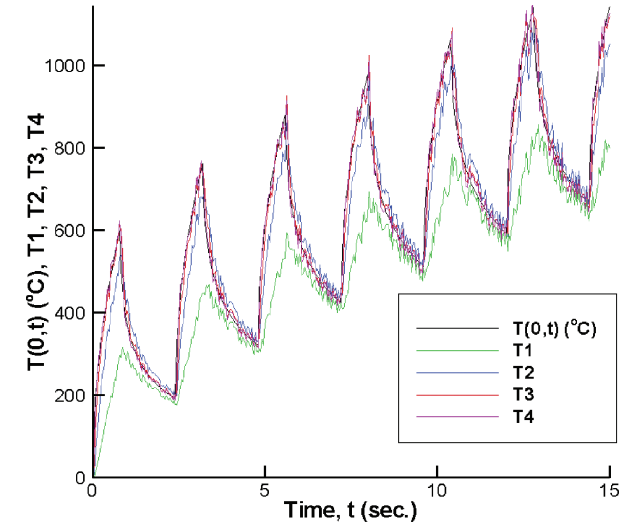

Fig. 8 Taylor approximation of $T(0, t)$ as additional terms are retained in the presence of noisy data, for iron: $\alpha = 2.3 \times 10^{-5}$ m^2/s, $k = 80.2$ W/(mK), $T_0 = 0°$C, and $\eta = 0.3175$ cm.

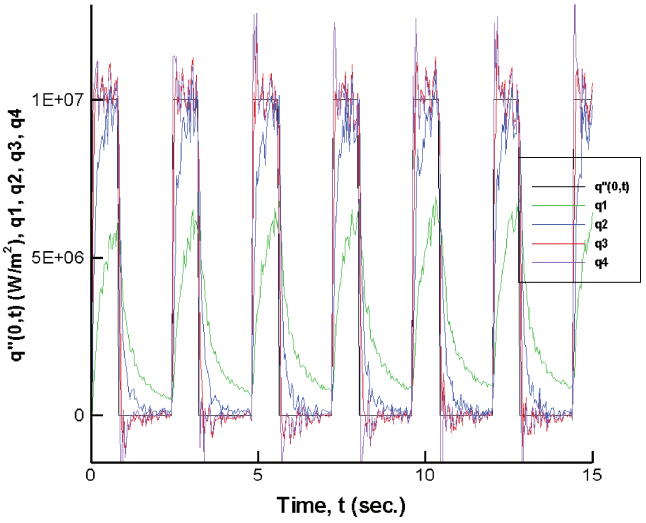

Fig. 9 Taylor approximation of $q''(0, t)$ as additional terms are retained in the presence of noisy data, for iron: $\alpha = 2.3 \times 10^{-5}$ m^2/s, $k = 80.2$ W/(mK), $T_0 = 0°$C, and $\eta = 0.3175$ cm.

and for the projected heat flux,

$$q''(0, t - t_{\text{pen}}) = q''(\eta, t) + \frac{k}{\alpha}\frac{\partial T}{\partial t}(\eta, t)\frac{\eta}{1!} + \frac{1}{\alpha}\frac{\partial q''}{\partial t}(\eta, t)\left(\frac{\eta^2}{2!} - t_{\text{pen}}\alpha\right) + \mathcal{O}(\eta^3) \tag{14b}$$

This consideration may become necessary under some circumstances.

As noted in Fig. 4, only five terms (T, q'', $\mathrm{d}T/\mathrm{d}t$, $\mathrm{d}q''/\mathrm{d}t$, and $\mathrm{d}^2T/\mathrm{d}t^2$) are needed to reconstruct the sawtooth-type surface temperature. This approach is equally valid on a finite width plate that is instrumented on the back surface, $x = \eta$. The errors are collected in an additive fashion as mandated by the Taylor series. This pulsed heat flux example represents a severe test condition for the concept.

Example 3: Classical Inverse Heat Conduction

A classical inverse heat conduction problem is now considered.[7,12,28] Inverse heat conduction involves the application of diffusion theory for estimating an unknown boundary condition, energy generation rates, or thermophysical properties through internally measured histories at one or more locations.[7,8] Typically, discrete data are obtained from embedded thermocouples. The natural questions arises as to whether these quantities are the most useful source of data for resolving ill-posed problems where stability is a critical issue.

Before proceeding further, the importance of heating/cooling rate data can be immediately displayed by merely changing the dependent variable of the field description from temperature to heat flux. This alternative viewpoint indicates that the projected heat flux is typically more difficult to reconstruct than the projected temperature. The conventional, linear, one-dimensional heat equation in temperature is

$$\frac{1}{\alpha}\frac{\partial T}{\partial t}(x, t) = \frac{\partial^2 T}{\partial x^2}(x, t), \qquad x \in (0, L), \qquad t > 0 \tag{15a}$$

subject to the one-sided boundary conditions

$$T(L, t) = f(t) \tag{15b}$$

$$-k\frac{\partial T}{\partial x}(L, t) = g(t), \qquad t > 0 \tag{15c}$$

and the uniform initial condition

$$T(x, 0) = T_0, \qquad x \in [0, L] \tag{15d}$$

For the moment, let the data functions $f(t)$, $g(t)$, and T_0 be specified functions or constants. This system can be equivalently expressed in heat flux as[29]

$$\frac{1}{\alpha}\frac{\partial q''}{\partial t}(x, t) = \frac{\partial^2 q''}{\partial x^2}(x, t), \qquad x \in (0, L), \qquad t > 0 \tag{15e}$$

subject to the one-sided boundary conditions

$$q''(L, t) = g(t) \tag{15f}$$

$$\frac{\partial q''}{\partial x}(L, t) = -\frac{k}{\alpha}\frac{\mathrm{d}f}{\mathrm{d}t}(t), \qquad t > 0 \tag{15g}$$

and the initial condition

$$q''(x, 0) = 0, \qquad x \in [0, L] \tag{15h}$$

where sufficient continuity is assumed at $t = 0$. This system is constructed using Fourier's law, $q'' = -k(\partial T/\partial x)$ and energy conservation $(k/\alpha)(\partial T/\partial t) = -(\partial q''/\partial x)$. Conversion back to temperature can be accomplished through the particular or general laws. Observe that Eq. (15g) requires the time derivative of the temperature (heating/cooling rate) to be specified to resolve for the heat flux. Here lies the crux of the inverse heat conduction problem.

The Beck et al. future information method[7] and Tikhonov regularization method (see Ref. 8) represent two conventional regularization techniques used by the heat transfer community. Both methods attempt to overcome numerical instability by different forms of regularization, and they both tend to remove high-frequency components in the solution space.

With the aid of the global time method,[28] a family of predictions is generated based on temperature data. To locate the optimal prediction from this family of solutions, a secondary set of data consisting of heating/cooling rate is used to isolate correctly the optimal prediction. It is well known in the study of inverse problems[12] that the numerical prediction implicitly depends on the differentiation of the data. Control or monitoring the heating/cooling rate term makes physical sense and can be exploited for acquiring optimal predictions.

A classical one-sided, one-dimensional, inverse heat conduction problem[7,12,28] is used to illustrate the impact of the auxiliary data set on assuring the determination of the optimal prediction. In particular, a plane-parallel medium is assume of dimensionless width two, where the spatial domain is defined by the region $\chi \in [-1, 1]$. The goal of the present inverse analysis involves predicting the surface heat flux and temperature at $\chi = -1$ when provided an overspecified set of boundary conditions at $\chi = 1$. This section follows the notation of Ref. 28, in which the computational/procedural approach required for obtaining the expansion coefficients, is described. The

constant property, dimensionless heat equation[12,28] can be expressed as

$$\frac{\partial^2\theta}{\partial\chi^2}(\chi,\xi)=\frac{1}{4\lambda_0}\frac{\partial\theta}{\partial\xi}(\chi,\xi),\qquad(\chi,\xi)\in[-1,1]\tag{16a}$$

where $\lambda_0=t_{\max}/2$. Here (χ,ξ) represent the Chebyshev spatial and temporal domains, $\theta(\chi,\xi)$ represents the dimensionless temperature, and $t_{\max}$ is the maximum Fourier time in the simulation. For the proposed inverse problem, the insulated condition at $\chi=1$ is given as

$$\frac{\partial\theta}{\partial\chi}(1,\xi)=0,\qquad\xi\in[-1,1]\tag{16b}$$

To form the one-sided inverse problem, the second specification contains the inexact, discrete temperature data given by

$$\theta(1,\xi_i)=\theta_i,\qquad i=1,2,\ldots,M\tag{16c}$$

Here, M represents the total number of measurements. The initial condition is given as

$$\theta(\chi,-1)=0,\qquad\eta\in[-1,1]\tag{16d}$$

In the present context, the desired dimensionless surface heat flux $Q(\xi)$ at $\chi=-1$ is mathematically expressed as

$$Q(\xi)=-2\frac{\partial\theta}{\partial\chi}(-1,\xi),\qquad\xi\in[-1,1]\tag{16e}$$

The classical Beck et al. triangular heat flux case[7] (see also Ref. 28) is considered. In this problem, numerically simulated discrete data are required at $\chi=1$. These data are obtained by assuming that a triangular heat flux is imposed at $\chi=-1$, whereas the back surface at $\chi=1$ is insulated. The exact solution is obtained for the local temperature $\theta(\chi,\xi)$ from which either simulated temperature or heating/cooling rate data are obtained at $\chi=1$. To reiterate, the goal is to reconstruct the triangular heat flux and surface temperature at $\chi=-1$ through a projection process.

The necessary discrete data are simulated with the aid of

$$\frac{\mathrm{d}^j\theta_i}{\mathrm{d}\xi^j}=\frac{\partial^j\theta}{\partial\xi^j}(1,\xi_i)+\sigma_j\,\mathrm{rand}_{j,i}\left\|\frac{\partial^j\theta}{\partial\xi^j}(1,\xi_i)\right\|_\infty$$
$$j=0,1,\qquad i=1,2,\ldots,M\tag{17}$$

The parameter σ_k, $k=0,1,2$, is a real-valued positive constant indicating the level of uncertainty, whereas the symbol $\mathrm{rand}_{k,i}$, $k=0,1,2$, is used to denote the returned value of a randomly drawn real number from the interval $[-1,1]$.

The global time method[12,28] uses a weighted-residual formalism where both the space and time variables are functionally represented. In particular, Hardy multiquadric radial-basis functions[30] are used in representing the time variable whereas Chebyshev polynomials of the first kind are used for representing the spatial variable. This method effectively mandates the use of all future and previous time information in the analysis through a continuous time representation. Regularization is achieved through temporal truncation. The expansion for this illustration takes the form

$$\theta(\chi,\xi)\approx\theta_{\mathrm{NP}}(\chi,\xi)=\sum_{m=1}^{N}\sum_{n=1}^{P}b_n^m\Omega_{mn}(\chi,\xi)\tag{18a}$$

for $(\chi,\xi)\in(-1,1)$, where

$$\Omega_{mn}(\chi,\xi)=\omega_m(\chi)\Big[\sqrt{\beta^2+(\xi-\xi_n)^2}-\sqrt{\beta^2+(1+\xi_n)^2}$$
$$+\sqrt{\beta^2}-\sqrt{\beta^2+(1+\xi)^2}\Big]\tag{18b}$$

$$\omega_m(\chi)=\begin{cases}1, & m=1\\ T_m(\chi)-\chi\dfrac{\mathrm{d}T_m}{\mathrm{d}\chi}(1), & m=2,3,\ldots,N\end{cases}\tag{18c}$$

where $T_m(\chi)$ represents the mth Chebyshev polynomial of the first kind. In time, Hardy multiquadric radial-basis functions are used having the shape factor $\beta^2=(2/P)$ and the centers defined by $\xi_n=-1+n/P$.

The procedure for determining the expansion coefficients can be found in Ref. 28. Because of the availability of the exact analytical solution, the projected surface temperature and heat flux squared-error norms are

$$\|\theta(-1,\xi)-\theta_{\mathrm{NP}}(-1,\xi)\|_2^2=\sum_{i=1}^{M}[\theta(-1,\xi_i)-\theta_{\mathrm{NP}}(-1,\xi_i)]^2\tag{19a}$$

$$\|Q(\xi)-Q_{\mathrm{NP}}(\xi)\|_2^2=\sum_{i=1}^{M}[Q(\xi_i)-Q_{\mathrm{NP}}(\xi_i)]^2\tag{19b}$$

Let the two-norm squared of the data approximation difference be defined as

$$N_j=\left\|\frac{\mathrm{d}^j\theta_i}{\mathrm{d}\xi^j}-\frac{\partial^j\theta_{\mathrm{NP}}}{\partial\xi^j}(1,\xi_i)\right\|_2^2=\sum_{i=1}^{M}\left[\frac{\mathrm{d}^j\theta_i}{\mathrm{d}\xi^j}-\frac{\partial^j\theta_{\mathrm{NP}}}{\partial\xi^j}(1,\xi_i)\right]^2$$
$$j=0,1\tag{20}$$

Observe that Eq. (19) involves true error metrics at the desired location ($\eta=-1$), whereas Eq. (20) defines metrics associated with differences between the data and approximation. In real cases, no exact solution is available. It is hoped that the minima of Eq. (20) over the P spectrum match the optimal predictions associated with Eq. (19). Consideration of higher-time derivatives for locating the optimal value of P yields similar results.[15] For the sake of graphical clarity, only up to the first derivative is considered in Eq. (20).

Figures 10 and 11 show simulated θ_i and $\dot\theta_i$ data, respectively, located at $\chi=1$. The numerically generated data make use of the exact solution at the corresponding probe point and add a random component in accordance to Eq. (17) to obtain the noisy data sets indicated by the dots in Figs. 10 and 11. Here, $\sigma_0=0.02$ and $\sigma_1=3\sigma_0$. The uncertainty level is intentionally increased to illustrate the robustness of the concept. The sampling is equidistant in time with $M=199$ and $\beta^2=2/P$. All solid lines represent exact solutions, dashed lines represent approximate solutions at the optimal prediction $P=p_{\mathrm{opt}}$, and open circles represent data.

Figures 12 and 13 illustrate the reconstructed projections using $P=p_{\mathrm{opt}}=7$ and $N=8$ and demonstrate excellent agreement with the exact solution. Figure 14 shows the error norms described in

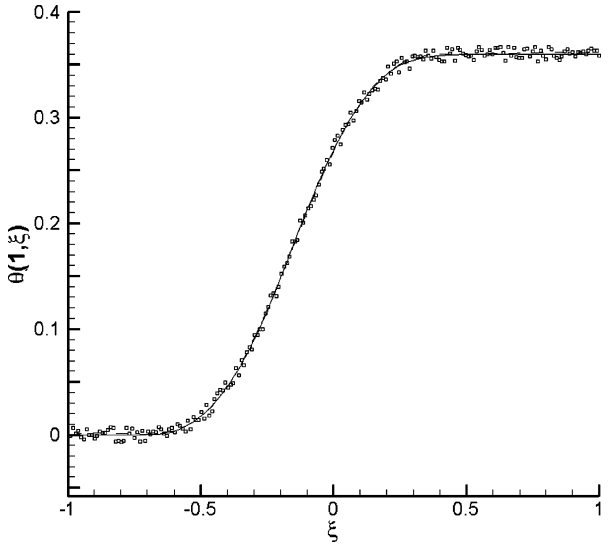

Fig. 10 Exact continuous temperature $\theta(1,\xi)$ and discrete, noisy temperature θ_i.

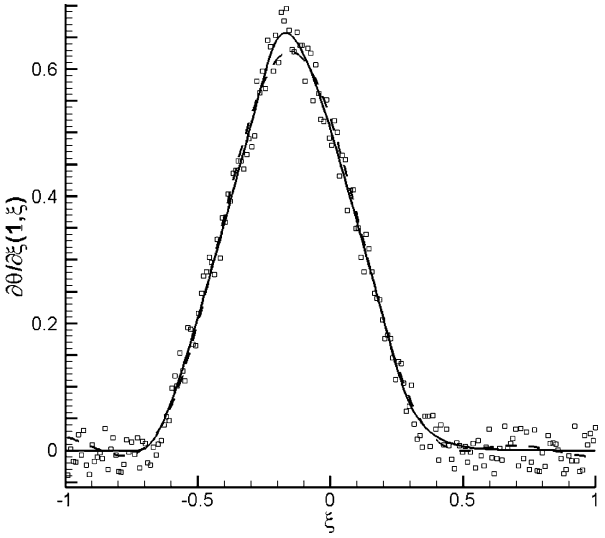

Fig. 11 Exact, continuous heating/cooling rate $(\partial\theta/\partial\xi)(1,\xi)$ and discrete, noisy heating/cooling rate data $\dot{\theta}_i$.

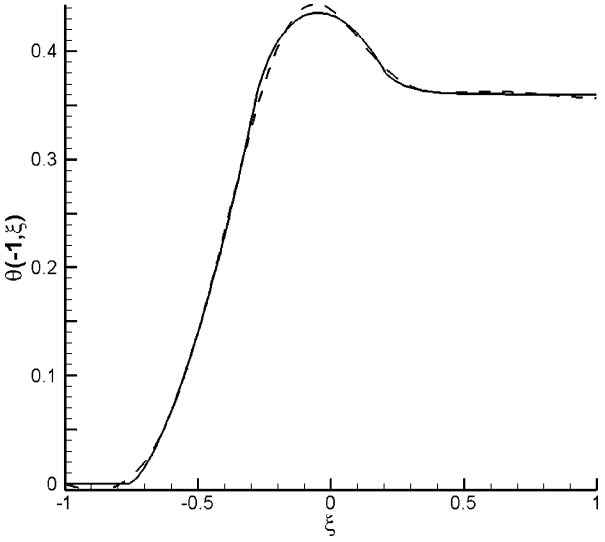

Fig. 12 Temperature: ——, exact $\theta(-1,\xi)$ and - - - -, reconstructed, $\theta_{\mathrm{NP}}(-1,\xi)$ when $P=7$.

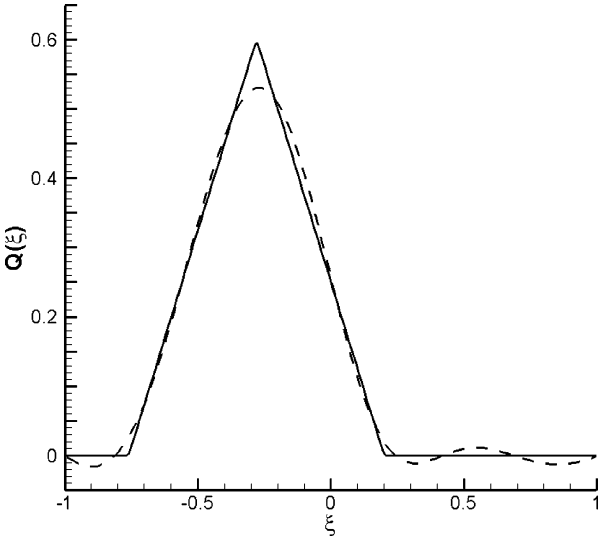

Fig. 13 Heat flux ——, exact $Q(\xi)$ and - - - -, reconstructed, $Q_{\mathrm{NP}}(\xi)$ when $P=7$.

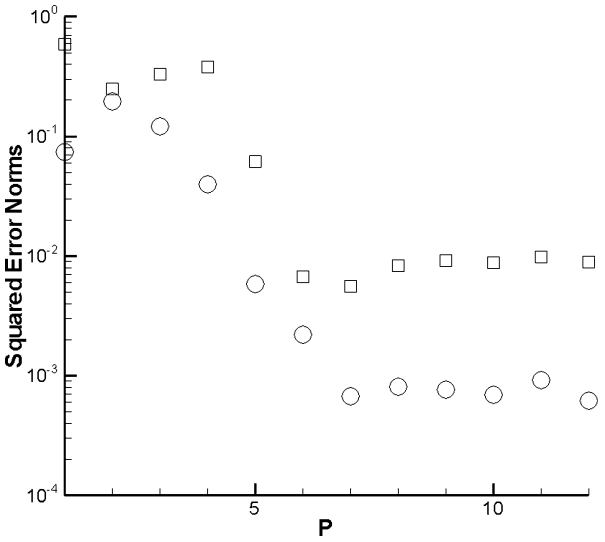

Fig. 14 Squared error norms over P spectrum: ○, temperature, Eq. (19a), and □, heat flux, Eq. (19b).

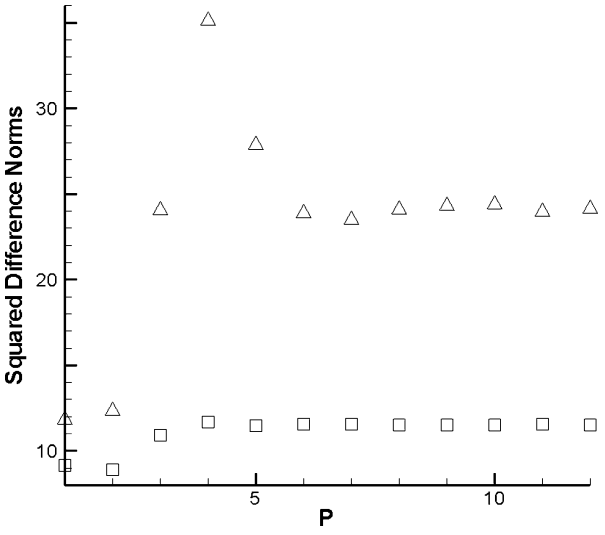

Fig. 15 Squared difference norms over P spectrum: □, temperature, Eq. (20), $j=0$, and △, heating/cooling rate, Eq. (20), $j=1$.

Eqs. (19a) and (19b), indicating that $P = p_{\mathrm{opt}} = 7$ is the optimal prediction at $\chi = -1$ for the corresponding surface temperature (open circles) and heat flux (open squares). Figure 15 presents the norms given in Eq. (20) for N_0 (open squares) and N_1 (open triangles). The first significant minimum of N_1 replicates the optimal value of 7. No significant insight is provided by N_0 due to lack of clarity. This is physically expected in light of the differential equation. From a lumped point of view, tracking N_1 over the P spectrum makes sense with regard to locating the optimal prediction for the surface heat flux.

Example 4: Moving Boundary-Value Problems with Embedded Sensors

This final example revisits the analytic continuation concept described in example 2, but extends it to include a moving surface.[31,32] The surface, denoted as $x = s(t) < L$, moves in the positive x direction due to some imposed thermal condition. Motion normally begins when the surface temperature exceeds the known (pure) melt temperature, T_{melt}. The Taylor series expansion of $T(x,t)$ about the embedded point $x = L > 0$, where $x \to s(t)$ and L is the fixed

location of the sensor array such that $0 < s^+(t) < x < L$, is

$$T[s(t),t] = T(L,t) - \frac{\partial T}{\partial x}(L,t)\frac{[L-s(t)]}{1!} + \frac{\partial^2 T}{\partial x^2}(L,t)\frac{[L-s(t)]^2}{2!} - \frac{\partial^3 T}{\partial x^3}(L,t)\frac{[L-s(t)]^3}{3!} + \frac{\partial^4 T}{\partial x^4}(L,t)\frac{[L-s(t)]^4}{4!}\cdots \quad (21)$$

when the procedure outlined in example 2 is followed, Eq. (21) can alternatively be expressed as

$$T[s(t),t] = T(L,t) + q''(L,t)\frac{[L-s(t)]}{1!k} + \frac{\partial T}{\partial t}(L,t)\frac{[L-s(t)]^2}{2!\alpha}, + \frac{\partial q''}{\partial t}(L,t)\frac{[L-s(t)]^3}{3!\alpha k} + \frac{\partial^2 T}{\partial t^2}(L,t)\frac{[L-s(t)]^4}{4!\alpha^2} + \cdots \quad (22)$$

when the availability of measured values is assumed for $T(L,t)$, $q''(L,t)$, $(\partial T/\partial t)(L,t)$, $(\partial q''/\partial t)(L,t)$, ..., permits the real-time reconstruction of the front location $s(t)$ because $T[s(t),t] = T_{\text{melt}}$. Thus, at any instant in time, the front location $s(t)$ is determined using a conventional root-finding method. When a similar Taylor series procedure is followed, the penetrating conductive heat flux becomes

$$q''[s(t),t] = q''(L,t) + \frac{k}{\alpha}\frac{\partial T}{\partial t}(L,t)\frac{[L-s(t)]}{1!} + \frac{1}{\alpha}\frac{\partial q''}{\partial t}(L,t)\frac{[L-s(t)]^2}{2!} + \frac{k}{\alpha^2}\frac{\partial^2 T}{\partial t^2}(L,t)\frac{[L-s(t)]^3}{3!} + \frac{1}{\alpha^2}\frac{\partial^2 q''}{\partial t^2}(L,t)\frac{[L-s(t)]^4}{4!} + \cdots \quad (23)$$

The heat flux penetrating the body is now determined by Eq. (23) because the front location $s(t)$ is known. The incident source is recovered from an overall energy balance at the regressing surface[31,32] (involving the latent heat of fusion, regression rate, and heat conduction into the body). A series of sensors could be distributed at various depths to account for lagging effects.

Conclusions

This paper conveys the need for the direct measurement or interpretation of higher-time derivatives of temperature and heat flux. The proposed hierarchal description is based on mathematical and physical observations. Temperature and heat flux sensors have been available for nearly a century. In the near future, preliminary results indicating how these quantitites can be measured are planned. Critical engineering applications that can take advantage of these alternative data types include the following: 1) rocket motor combustion, 2) reentry studies involving arcjets, 3) direct energy impingement, 4) fire analysis, and 5) quenching and distortion studies.

The development of heating/cooling rate sensors $\dot{T}$ (or even $\ddot{T}$) can be instrumental in determining a regularization parameter associated with inverse heat conduction. This concept actually takes advantage of the unsettling (growth, oscillation) solution behavior as the approximation level increases. That is, the cutoff in the numerical solution process is obtained by bounding it with an experimental quantity. Unstable growth in the temperature time derivative is not permitted. Physically, this energy consideration is consistent with the heat equation itself. Also, in-depth sensors can be utilized to monitor, in near real-time, occurrences taking place on a surface in a hostile environment. Health management issues involving control and feedback will certainly benefit by such an approach. This paper and its basic premises are presented in the spirit of motivation and to stimulate further intellectual discussions.

References

[1]Doebelin, E. O., *Measurement Systems*, McGraw–Hill, New York, 1975, Chap. 8.

[2]Diller, T. E., "Advances in Heat Flux Measurements," *Advances in Heat Transfer*, Vol. 23, Academic Press, New York, 1993, pp. 279–368.

[3]Lu, F. K., and Marren, D. E. (eds.), *Advanced Hypersonic Test Facilities*, Progress in Astronautics and Aeronautics, Vol. 198, AIAA, Reston, VA, 2002, pp. 279–314.

[4]Neumann, R. D., Erbland, P. J., and Kretz, L. O., "Instrumentation of Hypersonic Structures," AIAA Thermophysics, Plasmadynamics and Lasers Conf., June 1988.

[5]Kress, R., *Linear Integral Equations*, Springer-Verlag, Berlin, 1989, Chap. 15.

[6]Wing, G. M., *A Primer on Integral Equations of the First Kind*, Society for Industrial and Applied Mathematies, Philadelphia, 1991, Chap. 2.

[7]Beck, J. V., Blackwell, B., and St. Clair, C. R., Jr., *Inverse Heat Conduction*, Wiley, New York, 1985, Chap. 1.

[8]Kurpisz, K., and Nowak, A. J., *Inverse Thermal Problems*, Computational Mechanics, Southampton, U.K., 1995, Chap. 1.

[9]Hanke, M., and Scherzer, O., "Inverse Problems Light: Numerical Differentiation," *American Mathematical Monthly*, Vol. 108, June/July 2001, pp. 512–520.

[10]Groetsch, T., "Differentiation of Approximately Specified Functions," *American Mathematical Monthly*, Vol. 98, No. 9, 1991, pp. 847–850.

[11]Frankel, J. I., Keyhani, M., and Taira, K., "In-Phase Error Estimation of Experimental Data and Optimal First Derivatives," *AIAA Journal*, Vol. 42, No. 5, 2004, pp. 1017–1024.

[12]Frankel, J. I., and Keyhani, M., "Inverse Heat Conduction: The Need of $\partial T/\partial t$ Data for Design and Diagnostic Purposes," Paper 113, International Conference on Modeling, Identification and Controls, International Association of Science and Technology for Development, Feb. 1999.

[13]Frankel, J. I., "Inverse Heat Conduction and Data-Type Issues," *Boundary Element Communications*, Vol. 11, No. 4, 2000, pp. 37–42.

[14]Frankel, J. I., and Osborne, G. E., "The Development of Heating/Cooling Rate, dT/dt and Heat Flux Rate, dq″/dt Sensors for Aerospace Applications," Propulsion Measurement Sensor Development Workshop, Paper 1.2.4, NASA, Huntsville, AL, May 2003.

[15]Frankel, J. I., and Osborne, G. E., "The Prediction of Heating/Cooling Rates in Material Science Investigations," 4th International Conference on Quenching and Control of Distortion, Paper 86, Chinese Heat Treatment Society, Beijing, PRC, Nov. 2003.

[16]Frankel, J. I., and Osborne, G. E., "Motivation for the Development of Heating/Cooling Rate dT/dt and Heat Flux Rate dq"/dt Sensors for Engineering Applications," AIAA Paper 2004-0823, Jan. 2004.

[17]Lu, F. K., and Kinnear, K. M., "Characterization of Thin Film Heat-Flux Gauges," 20th Advanced Measurement and Ground Testing Technology Conf., AIAA Paper 98-2504, June 1998.

[18]Hodge, J. K., Chen, A. L., and Hayes, J. R., "Unsteady Heat Transfer Coefficient Estimation for Long Duration," *Journal of Thermophysics and Heat Transfer*, Vol. 2, No. 3, 1988, pp. 218–226.

[19]Cook, W. J., and Felderman, E. J., "Reduction of Data from Thin-Film Heat Transfer Gauges: A Concise Numerical Technique," *AIAA Journal*, Vol. 4, March 1966, pp. 561–562.

[20]Cook, W. J., "Determination of Heat Transfer Rates from Transient Surface Temperature Measurements," *AIAA Journal*, Vol. 8, No. 7, 1970, pp. 1366–1368.

[21]Linz, P., *Analytical and Numerical Methods for Volterra Equations*, Society for Industrial and Applied Mathematics, Philadelphia, 1985, Chap. 8.

[22]Baker, C. T. H., *The Numerical Treatment of Integral Equations*, Clarendon Press, Oxford, England, U.K., 1978, Chap. 6.

[23]Golberg, M. A. (ed.), *Solution Methods for Integral Equations*, Plenum, New York, 1979, Chap. 1.

[24]Ozisik, M. N., *Heat Conduction*, Wiley, New York, 1980, Chap. 1.

[25]Arpaci, V. S., *Conduction Heat Transfer*, Addison Wesley Longman, Reading, MA, 1966, Chap. 1.

[26]Brebbia, C. A., Telles, J. C. F., and Wrobel, L. C., *Boundary Element Techniques*, Springer-Verlag, Berlin, 1984, Chap. 4.

[27]Kaplan, W., *Advanced Calculus*, 2nd ed. Addison Wesley Longman, Reading, MA, 1973, p. 439.

[28]Frankel, J. I., and Keyhani, M., "A Global Time Treatment for Inverse Heat Conduction Problems," *Journal of Heat Transfer*, Vol. 119, Nov. 1997, pp. 673–683.

[29]Frankel, J. I., Vick, B., and Ozisik, M. N., "Flux Formulation in Hyperbolic Heat Conduction," *Journal of Applied Physics*, Vol. 58, No. 9, 1985, pp. 3340–3345.

[30]Hardy, R. L., "Theory and Applications of the Multiquadric Biharmonic Method," *Computers in Mathematics with Applications*, Vol. 19, No. 8, 9, 1990, pp. 163–208.

[31]Boley, B. A., and Weiner, J. H., *Theory of Thermal Stresses*, Dover, New York, 1997, Chap. 6.

[32]Penner, S. S., and Olfe, D. B., *Radiation and Reentry*, Inst. for Defense Analysis, Washington, DC, 1968, Chap. 7.